



## Scenario tree and adaptive decision making on optimal type and timing for intervention and social-economic activity changes to manage the COVID-19 pandemic

K. Nah<sup>1</sup>, S. Chen<sup>2</sup>, Y. Xiao<sup>3</sup>, B. Tang<sup>1</sup>, N. L. Bragazzi<sup>1</sup>, J. M. Heffernan<sup>1,4</sup>, A. Asgary<sup>5</sup>, N. H. Ogden<sup>6</sup>, J. Wu<sup>1,\*</sup>

<sup>1</sup> *Laboratory for Industrial and Applied Mathematics, Department of Mathematics and Statistics, York University, Toronto, Ontario, Canada*

<sup>2</sup> *Department of Mathematics and Statistics, York University, Toronto, Ontario, Canada*

<sup>3</sup> *Department of Mathematical Sciences, University of Cincinnati, Cincinnati, OH, USA*

<sup>4</sup> *Modelling Infection and Immunity Lab, Centre for Disease Modelling, Department of Mathematics and Statistics, York University, Toronto, Ontario, Canada*

<sup>5</sup> *Disaster & Emergency Management, School of Administrative Studies & Advanced Disaster & Emergency Rapid-response Simulation (ADERSIM), York University, Toronto, Ontario, Canada*

<sup>6</sup> *Public Health Risk Sciences Division, National Microbiology Laboratory, St-Hyacinthe/Guelph Public Health Agency of Canada, Guelph, Canada*

---

**Abstract.** We introduce a novel approach to inform the re-opening plan followed by a post-pandemic lockdown by integrating a stochastic optimization technique with a disease transmission model. We assess Ontario's re-opening plans as a case-study. Taking into account the uncertainties in contact rates during different re-opening phases, we find the optimal timing for the upcoming re-opening phase that maximizes the relaxation of social contacts under uncertainties, while not overwhelming the health system capacity before the arrival of effective therapeutics or vaccines.

**2020 Mathematics Subject Classifications:** 92D30, 90C15, 37N40

**Key Words and Phrases:** Scenario tree, COVID-19 social distancing, lockdown exit strategy, re-opening, transmission dynamics model, stochastic optimization

---

### 1. Introduction and Background

Planning re-opening after several phases of social distancing escalation in order to manage the Coronavirus disease 2019 (COVID-19) pandemic has been challenging for policy- and decision-makers globally. Re-opening too soon could cause an immediate local resurgence; re-opening too late would lead to huge unnecessary economic losses and other

---

\*Corresponding author.

DOI: <https://doi.org/10.29020/nybg.ejpam.v13i3.3792>

Email address: [wujh@yorku.ca](mailto:wujh@yorku.ca) (J. Wu)

adverse effects on health. Most governments around the world have adopted a stage-wise re-opening strategy, in which different social-economic activities are permitted in different stages while the epidemic is closely monitored to ensure the needs for intensive care units (ICU) beds and other medical resources do not exceed the health system capacity.

COVID-19 transmission dynamic models [18, 20, 22–24] have been used to estimate the peak demand of ICU beds. These models, however, have ignored the inherent stochasticity in nature and human behaviour (i.e., contact rates) that will affect future social distancing relaxation stages, which will ultimately affect the magnitude and timing of the epidemic peak in future outbreak scenarios, including ICU bed needs. This uncertainty poses great challenges to public health decision- and policy-makers in the design, i.e., timing, type of change, that future phases of re-opening of the economy should include. To meet these challenges, here we develop a quantitative stochastic programming model to support a multi-stage decision-making process under substantial uncertainty.

Our key idea is to make the best possible decision in re-opening given currently available information that may be weak. Such available weak information is provided by a disease transmission dynamical system that incorporates intrinsic uncertainty in individual behavior, resulting in randomness of the daily average contact rate. Indeed, the exact contact rate for different future stages of re-opening are not known. However, they can be informed by, for example, mathematical modelling studies of historical measures of COVID-19 public health mitigation strategies during different closure stages – bounds of contact rates in the future may be reasonably established in terms of the economic sector and social, economic and health considerations, from which ranges in the timing and magnitude of peak demand of ICU units can be inferred. Furthermore, we can consider different scenarios of the contact rate distributions. Consequently, the distribution of peak demands can be established as well. This provides a scientific basis to calculate the expected loss of contacts, rather than considering only the worst- and/or best-case scenario. A natural approach is to calculate the peak demand based on the average of the future contact rate, however the dynamics of the disease transmission renders dependence of the peak demand on the contact rate highly nonlinear, and it is known that the expectation of a nonlinear function of a random variable is in general different from the nonlinear function of the expectation of the random variable.

A critical consideration in re-opening is the recourse option. It is possible that, once re-opened, or when re-opening is initiated, outcomes may be worse than expected, and corrective actions must be taken. A complete re-implementation of lockdown would be the safest solution, but in the long-term it is not acceptable, feasible or sustainable. We, therefore, must consider re-opening plans that allow for some variability in outcomes so that severe recourse actions will not be needed. In this type of multistage decision problem, the first stage decision shall therefore leave enough room for future recourse in unfavourable cases. An aggressive first stage decision might lead to a better result in a favorable case, but could cause failure in an unfavourable one. On the other hand, a pessimistic first stage decision incurs very high social-economic costs. An optimal first stage decision shall take into account the recourse options and the distribution of future uncertainties, and therefore, will yield a proactive and reactive re-opening policy. The

policy is not the best in the favorable case, and is not the best in the worst case either, but it is overall optimal in a holistic sense.

Here we develop a stochastic programming model based on an adopted disease transmission dynamical system [18]. The model formulation and its numerical simulations take full consideration of: (1) the adaptive decision process; (2) the contact rate uncertainties; (3) recourse actions and consequences; and (4) the underlying dynamics of COVID-19 which is described by an ODE system. Stochastic programming is a well established model and is widely used in finance, transportation, agriculture, etc., see [23]. To our best knowledge, this is the first attempt to integrate stochastic optimization and disease transmission models for informing re-opening optimal strategies. It is also innovative in that it is the synthesis of an underlying dynamical process described by a disease transmission model involving other public health interventions.

In our numerical simulations, we take the province of Ontario, Canada, as a case study. The optimal re-opening plan is achieved by maximizing the total activities from the beginning of the re-opening process to an assumed date when an effective therapeutics or vaccine against COVID-19 is available, subject to the capacity of the health system and the uncertainties of contact rates during the re-opening phases. Using the tools of stochastic programming and the disease transmission model, we find optimal timings for each re-opening phase, that maximizes the relaxation of social contacts under uncertainties while not overwhelming the health system, awaiting the arrival of an effective SARS-CoV-2 therapeutics or vaccine.

## 2. Materials and Methods

### 2.1. The Transmission Dynamics Model

We use a compartmental model describing COVID-19 transmission dynamics that incorporates feasible public health measures, including detection of cases by testing and their isolation, and tracing of contacts with cases and their quarantine. In the model formulation, the population is divided into susceptible ( $S$ ), exposed ( $E$ ), asymptomatic infectious ( $A$ ), infectious with symptoms ( $I$ ), and recovered ( $R$ ) compartments according to the clinical-epidemiological status of individuals. We also include diagnosed and isolated ( $D$ ), isolated susceptible ( $S_q$ ), and isolated exposed ( $E_q$ ) compartments based on control interventions. Within the modelling framework, we take contact tracing into account, where a proportion,  $q$ , of individuals exposed to the virus are traced and isolated (referred to as the quarantine proportion). Quarantined individuals can either move to the compartment  $E_q$  or  $S_q$ , depending on whether transmission has occurred (with probability  $q$ ), while the other proportion,  $1 - q$ , consists of individuals exposed to the virus who are missed from contact tracing and, therefore, move to the exposed compartment  $E$  if infected, or stay in

the compartment  $S$  otherwise. The transmission dynamics model is

$$\begin{aligned}
 S' &= -\beta c + cq(1 - \beta)S(I + \theta A)/N + \lambda S_q, \\
 E' &= \beta c(1 - q)S(I + \theta A)/N - \sigma E, \\
 I' &= \sigma \rho E - (\delta_I + \alpha + \gamma_I)I, \\
 A' &= \sigma(1 - \rho)E - \gamma_A A, \\
 S'_q &= (1 - \beta)cqS(I + \theta A)/N - \lambda S_q, \\
 E'_q &= \beta cqS(I + \theta A)/N - \delta_q E_q, \\
 D' &= \delta_I I + \delta_q E_q - (\alpha + \gamma_D)D, \\
 R' &= \gamma_I I + \gamma_A A + \gamma_D D,
 \end{aligned} \tag{1}$$

where  $N$  denotes the total population. The model was developed in a series of studies, and parameterized by fitting to the incidence data in a number of settings including the first reported epicenter Wuhan [17, 19, 21], in other provinces in China [20], in South Korea [20], in Italy [14] and in the Province of Ontario, Canada [18, 24]. In what follows, we will use the model fitted to the incidence data in Ontario, however, the model structure and optimization techniques we develop here can be applied to other settings and regions.

In order to develop optimal strategies to gradually relax the social distancing subject to key medical resources (hospital wards, ICU beds, for example), we divide compartment  $D(t)$  (those diagnosed but not-yet-recovered individuals) as follows:

$$D = D_{mild} + D_{ICU} + D_{ward}.$$

In other words, we distinguish the confirmed cases into those who show only mild symptoms and do not require hospitalization ( $D_{mild}$ ), those who are hospitalized in the ICU with severe symptoms ( $D_{ICU}$ ), and those who are hospitalized in non-ICU units ( $D_{ward}$ ). The disease progression and medical treatment process is described as follows:

$$\begin{aligned}
 D'_{mild} &= (1 - h)(\delta_I I + \delta_q E_q) - (\alpha + \gamma_{mild})D_{mild}, \\
 D'_{ICU} &= h(1 - w)(\delta_I I + q E_q) + b_{ward} D_{ward} - (\alpha + \gamma_{ICU})D_{ICU}, \\
 D'_{ward} &= hw(\delta_I I + \delta_q E_q) - (\alpha + \gamma_{ward} + b_{ward})D_{ward}.
 \end{aligned} \tag{2}$$

Here,  $h$  is the proportion of hospitalized cases among newly confirmed cases, among which a proportion  $w$  are hospitalized in non-ICU units directly. In our simulations and analyses, we use values of  $h$  and  $w$  estimated in [2], namely,  $h = 0.16$  and  $w = 0.77$ . The recovery rates for individuals in each state are denoted by mild, ICU and ward. Here, we use values from [10, 15, 16], namely,  $\gamma_{mild} = 1/5$ ,  $\gamma_{ICU} = 1/14$  and  $\gamma_{ward} = 1/12$ . The value of  $b_{ward}$  we will use is estimated to be  $0.26 \times \frac{1}{3}$  which is the product of two quantities: the proportion of patients who are moving to ICU beds among those who are originally admitted to non-ICU units, 0.26 [22], and the average duration of the pre-ICU period of 3 days [22].

Specifically, after March 2, the model was used to determine a time varying contact rate  $c(t)$  and quarantine proportion  $q(t)$ , that were assumed to be exponentially decreasing and increasing with exponential rates  $r_1$  and  $r_2$ , respectively. That is, by introducing  $T_0$ ,  $T_1$  and  $T_s$  corresponding to March 14 (School closure began), March 18 (Emergency declaration,

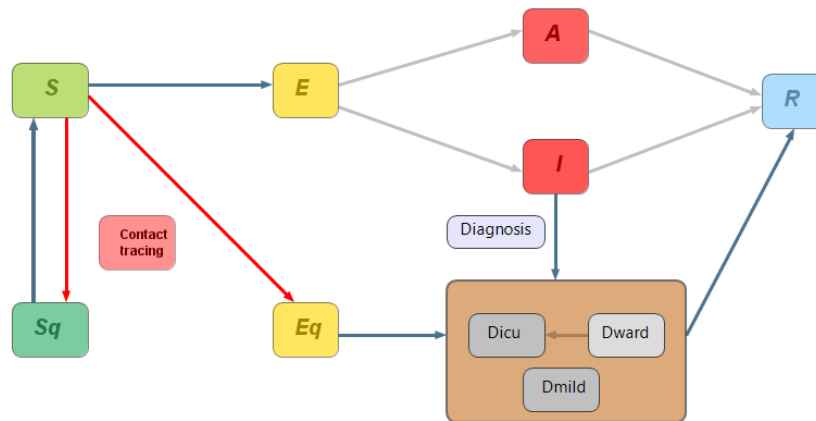


Figure 1: The flowchart of the transmission dynamics model, where the population is stratified by susceptible ( $S$ ), exposed ( $E$ ), asymptomatic infectious ( $A$ ), symptomatic infectious ( $I$ ), and recovered status ( $R$ ), and by quarantine and isolation status (i.e.  $S_q$  and  $E_q$ ). The compartment of diagnosed but not yet resolved cases is further stratified by the need for the use of hospital wards ( $D_{ward}$ ) and/or ICU beds ( $D_{ICU}$ ), and mild ( $D_{mild}$ ).

with closure of public events and recreational venues; Escalation), and March 24 (Closure of all non-essential workplaces), respectively, a full parameterization of the model for each phase of the escalation process in Ontario, Canada was determined (see [18]). Table 1 contains the values of parameters used for the simulation. Parameters estimated from [18] are presented with standard deviations.

## 2.2. Stochastic Optimization of De-escalation Plans

We investigate a social distancing de-escalation plan in which the escalation process experienced in the Province Ontario is reversed through a staged approach. Therefore, four main de-escalation phases will be considered:

- De-escalation-Phase 0 and 1: Opening of workplaces;
- De-escalation-Phase 2: Resumption of public events and activities;
- De-escalation-Phase 3: School opening.

We set up the initiation time of de-escalation phase 0 to be May 19, the first day of the (partial) workplace re-opening. We look for the optimal initiation time of de-escalation phase 1, 2 and 3 while keeping the number of diagnosed cases below a certain threshold. This threshold is set by the health system capacity, especially the number of ICU beds in the province. We aim to minimize the reduction in contacts compared to the contacts of the pre-pandemic level until an expected arrival time of a COVID-19 therapeutics or vaccine, assumed, herewithin, to be January 2021. In the final discussion section, we discuss how our approach can be modified to obtain results subject to different assumptions on public health measures and the arrival time of vaccines. We aim to find the optimal de-escalation strategy (the optimal time to switch between contact rates) within the health system capacity, taking into account the various scenarios of social-economic activities at each de-escalation phase. We emphasize that in our study, we assume that the contact rates at each de-escalation phase (1, 2, and 3) are random variables.

Table 1: Parameters for COVID-19 transmission dynamics in Ontario, Canada.

Parameter	Definition	Mean (STD)
$c_0$	Contact rate before March 14	11.5801 (0.3456)
$c_1$	Contact rate between March 14 to March 18	10.1202 (0.9185)
$c_2$	Contact rate between March 18 to March 24	8.0495 (0.2787)
$r_1$	Exponential decrease of contact rate	0.0466 (0.0152)
$c_b$	Minimum contact rate after March 24	2.1987 (0.2400)
$\beta$	Probability of transmission per contact	0.1469 (0.0023)
$q_0$	Fraction of quarantined exposed individuals before March 24	0.1145 (0.0114)
$r_2$	Exponential increase of quarantine fraction	0.1230 (0.0123)
$q_b$	The maximum quarantine fraction	0.3721 (0.0371)
$\sigma$	Transition rate of exposed individuals to the infected class	1/5
$\lambda$	Rate at which the quarantined uninfected contacts were released into the wider community	1/14
$\rho$	Probability of having symptoms among infected individuals	0.7036 (0.0261)
$\delta_I$	Transition rate of symptomatic infected individuals to the quarantined infected class	0.1344 (0.0134)
$\delta_q$	Transition rate of quarantined exposed individuals to the quarantined infected class	0.1237 (0.0086)
$\gamma_I$	Recovery rate of symptomatic infected individuals	0.1957 (0.0111)
$\gamma_A$	Recovery rate of asymptomatic infected individuals	0.139
$\gamma_{mild}$	Recovery rate of diagnosed individuals with mild symptoms	0.2
$\gamma_{ICU}$	Recovery rate of individuals in ICU units	1/14
$\gamma_{ward}$	Recovery rate of individuals in non-ICU units	1/12
$\alpha$	Disease-induced death rate	0.008
$\theta$	Modification factor of asymptomatic infectiousness	0.0275 (0.0128)
$h$	Proportion of hospitalized cases among newly confirmed cases	0.16
$w$	Proportion of cases admitted to non-ICU units among newly hospitalized cases	0.77
$b_{ward}$	Rate of transfer from non-ICU units to ICU units	$0.26 \times \frac{1}{3}$
Initial values	Definition	Mean (STD)
$S(0)$	Initial susceptible population	1.471107
$E(0)$	Initial exposed population	8.9743 (0.6558)
$I(0)$	Initial symptomatic infected population	5.3887 (0.9442)
$A(0)$	Initial asymptomatic infected population	19.4186 (3.9406)
$S_q(0)$	Initial quarantined susceptible population	0
$E_q(0)$	Initial quarantined exposed population	0
$D_{mild}(0)$	Initial diagnosed population with mild symptom	4
$D_{ICU}(0)$	Initial diagnosed population in ICU units	0
$D_{ward}(0)$	Initial diagnosed population in non-ICU units	1
$R(0)$	Initial recovered population	0

We consider four time-points,  $t_0, t_1, t_2$  and  $t_3$ , each of which corresponds to the first re-opening date of some workplaces (May 19, 2020), de-escalation-phase 1, de-escalation-phase 2 and de-escalation-phase 3. Each de-escalation phase is characterized by a contact rate, with  $c_{r,0}, c_{r,1}, c_{r,2}$  and  $c_{r,3}$  denoting the contact rates in each de-escalation phase

Table 2: Parameters for COVID-19 transmission dynamics post-re-opening in Ontario, Canada.

Parameter	Definition	Value
$c_p$	Contact rate between April 22 and May 19	4.5191
$c_{r,0}$	Contact rate during de-escalation phase 0 (since May 19)	5.3736
$[c_{r,1}, \overline{c_{r,1}}]$	Range of the contact rate during de-escalation phase 1	[6, 9.394]
$[c_{r,2}, \overline{c_{r,2}}]$	Range of the contact rate during de-escalation phase 2	[9.394, 10.5]
$[c_{r,3}, \overline{c_{r,3}}]$	Range of the contact rate during de-escalation phase 3	[10.5, 11.58]
$q_r$	Quarantine fraction after re-opening (since May 19)	0.3741
$\delta_{I,r}$	Transition rate of symptomatic infected individuals to the quarantined infected class after re-opening (since May 19)	0.1586
$\beta_r$	probability of transmission per contact (since May 19)	0.13

(0, 1, 2 and 3). Symmetric triangular distributions are defined on the ranges presented in Table 2. We set up the maximum level of contact rate to be the one at the pre-pandemic level and assume that  $\overline{c_{r,3}} = 11.58$ . The ranges of each triangular distribution are chosen from [25]. They are calculated by modifying weights of four different contact matrices at households, workplaces, schools and communities and others according to strategies of relaxing social distance in different de-escalation phases in Ontario, Canada. In [25], we used age- and location-specific contact matrices to calculate the average total contact rate (per day) during different phases of COVID-19 mitigation in Ontario, Canada. Using the transformations between different populations developed in [3], we calculated the contact matrix for Ontario, Canada based on the POLYMOD 2015s survey data ([11, 13]) for Canada. We then constructed contact matrices for four different location settings: households, workplaces, community-and-others, and schools among 18 age groups. These age groups have different daily schedules during weekdays and weekend, for example, young kids may go to daycares, students go to primary schools, high schools and colleges, working adults and seniors go to work during the weekdays. Assuming the overall contact mixing is a function of the four baseline matrices, base on possible age groups-specific schedules, we calculated different weights for these four baseline matrices from May 19, 2020 for the three de-escalation phases.

In order to obtain the contact rate  $c_{r,0}$ , the quarantine rate  $q_r$  and case detection rate  $\delta_{I,r}$  post re-opening (i.e. after May 19), we have first fixed all the other parameter values (all the parameters are constants) to those estimated in the previous study [18]. Note that, we also introduced a new parameter  $c_p$  describing the contact rate during the pre-re-opening stage (i.e. April 22 to May 19) as the estimation in the previous study [18] only used the data till April 21. Using the least square method, we fitted the model to the data of cumulative reported cases between April 22 to June 9 in Ontario, where the initial conditions (i.e. April 22) are obtained by solving the model in the previous study [18] based on the estimated parameter values. The estimated values for  $c_p, c_{r,0}, q_r, \delta_{I,r}$  are displayed in Table 2. Further, the transmission probability after re-opening is assumed to be lower than that of the pre-re-opening stage ( $\beta_r > \beta$ ) due to increased use of PPE (masks) by the public and personal distancing. The estimate of  $\beta_r$  is taken from the result of the similar modeling study in China [20].

We consider the acceptable de-escalation strategies which meet the constraints

$$D_{ICU}(t) \leq \underline{D}_{ICU} \quad \text{for } t_0 < t < t_0 + T,$$

where,  $t_0 + T$  is the time corresponding to the end of cost-evaluation and  $\underline{D}_{ICU}$  is a capacity of the ICU beds available for COVID-19 patients. The total number of existing ICU and acute beds in Ontario, Canada as of April 16, 2020 is 3504 and 20,354, respectively [1]. We assume that only a portion of these resources is available for COVID-19 patients.

A de-escalation strategy refers to the vectors  $(\epsilon_0, \epsilon_1, \epsilon_2)$  determined by  $\epsilon_i = t_{i+1} - t_i$ , for  $i = 1, 2, 3$ . Here,  $\epsilon_0$  represents the length of de-escalation phase 0 starting from  $t_0$  (May 19), 1, 2 and 3 are the duration of the de-escalation phases 1, 2 and 3, respectively. The initiation time of de-escalation phase 3 is at the time  $t_3 = t_2 + \epsilon_2$ . Note that  $\epsilon_3$  is determined by the equation  $\epsilon_0 + \epsilon_1 + \epsilon_2 + \epsilon_3 = T$  and we denote a de-escalation strategy corresponding to the scenario  $(c_{r,1}^j, c_{r,2}^j, c_{r,3}^j)$  to be  $(\epsilon_0^j, \epsilon_1^j, \epsilon_2^j)$ . We consider the situation that re-opening phases are separated by at least two weeks so that the minimal 2 weeks phase switching time is assumed  $\epsilon_i \geq 14$ , for  $i = 0, 1, 2$ . The days of cost-evaluation are set so that the end of the evaluation time corresponds to January 2021.

We solve the following scenario based stochastic programming model [4] to minimize the intensity of reduced contacts (cost) during de-escalation phases 0, 1, 2 and 3,

$$\sum_j w^j \left( \sum_{i=0}^3 (\bar{c}_{r,3} - c_{r,i}^j) \epsilon_i^j + ug(\epsilon_0^j, \epsilon_1^j, \epsilon_2^j) \right),$$

where

$$g(\epsilon_0^j, \epsilon_1^j, \epsilon_2^j) = -\log(\underline{D}_{ICU} - \max_{t_0 < t < t_0 + T} D_{ICU}(t)),$$

$u$  is set to  $10^{-6}$ ,  $w^j$  are the likelihood of scenarios. All constraints mentioned above, especially the transmission dynamic model, are included in the above scenario based stochastic programming model. Furthermore, all decision variables are subject to the non-anticipativity constraints [4] so as to generate a recourse solution, in which  $\epsilon_0$  is made before any uncertainty is revealed,  $\epsilon_1^j$  are made after  $c_{r,1}^j$  is observed and is adapted to it, and  $\epsilon_2^j$  are made after both  $c_{r,1}^j$  and  $c_{r,2}^j$  are observed and is adaptive as well. In a way,  $c_{r,3}^j$  are not included in the non-anticipative conditions, however, they change the value of the cost function and therefore also change the optimal strategy. Hence  $\epsilon_0$  part of the resource solution is immediately implementable by the policy maker, while  $\epsilon_1^j$  and  $\epsilon_2^j$  are path dependent, providing solutions to all possible future cases present in the model. The solution suite covers favorable cases, as well as unfavorable cases. The decision model incorporates uncertainty and models the adaptive decision process.

The scenario-based model is then implemented in a rolling horizon scheme, i.e., we solve the model and implement the optimal  $\epsilon_0$  right away, and near the end of  $\epsilon_0$ , we solve the model with new information collected during  $\epsilon_0$ , such as the actual system status and updated distribution of involved random variables, etc. The updated model will yield a new  $\epsilon_0$  to be implemented at that time. Though the  $\epsilon_1^j$  and  $\epsilon_2^j$  are never implemented, their existence show that the  $\epsilon_0$  being implemented won't lead to any future infeasibility for any scenario considered in the model.

### 3. Results

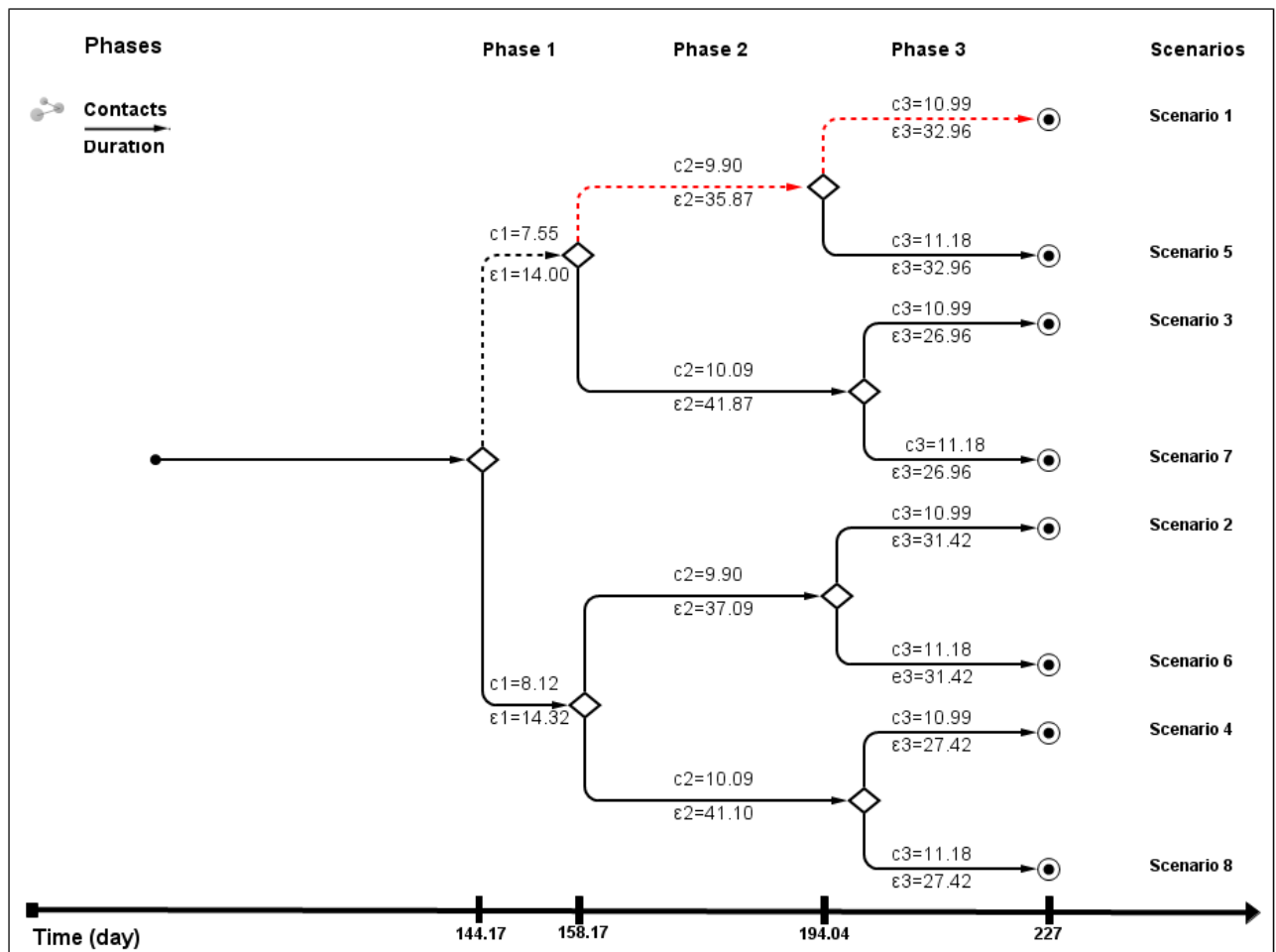


Figure 2: A scenario tree with 8 scenarios presented in Table 3. The date of vaccine arrival time is assumed to be in January 2021.

Fig. 2 and Table 3 present the optimal de-escalation strategy considering 8 different scenarios of the contact rates during 3 de-escalation phases,  $(c_{r,1}^j, c_{r,2}^j, c_{r,3}^j)$ ,  $j = 1, \dots, 8$ . The resulting duration of de-escalation phase 0 is approximately 144 days ( $\epsilon_0 = 144.17$  (days)). The optimal lengths of de-escalation phase 1 are close to the minimum length,  $\epsilon_1 = 14$  (days), while the length of de-escalation phase 2 ( $\epsilon_2$ ) varies from approximately 35 days to 42 days, depending on the scenario.

As shown in Fig. 3, while the expected cases in ICU units remain to be less than the capacity by the time of therapeutics/vaccine availability, the number of symptomatic infected cases ( $I(t)$ ) and asymptomatic infected cases ( $A(t)$ ) will exceed the capacity of ICU beds at the end of December, a few days prior to the therapeutics/vaccine arrival time. We also observe that regardless of the choice of the scenario, the solution curves for

Table 3: Optimal de-escalation strategies considering various scenarios for de-escalation phase 0, 1, 2 and 3. Each of the  $\epsilon_1, \epsilon_2, \epsilon_3$  and  $\epsilon_4$  represents the duration (in days) of de-escalation phase 0, 1, 2 and 3, respectively. Calendar dates presented in the rows of  $t_1, t_2, t_3$  correspond to the date of initiating de-escalation phase 1, 2 and 3, in the year of 2020.

	$s_1$	$s_2$	$s_3$	$s_4$	$s_5$	$s_6$	$s_7$	$s_8$
$c_{1,r}$	7.55	8.12	7.55	8.12	7.55	8.12	7.55	8.12
$c_{2,r}$	9.90	9.90	10.09	10.09	9.90	9.90	10.09	10.09
$c_{3,r}$	10.99	10.99	10.99	10.99	11.18	11.18	11.18	11.18
$\epsilon_0$	144.17	144.17	144.17	144.17	144.17	144.17	144.17	144.17
$\epsilon_1$	14.00	14.32	14.00	14.32	14.00	14.32	14.00	14.32
$\epsilon_2$	35.87	37.09	41.87	41.10	35.87	37.09	41.87	41.10
$\epsilon_3$	32.96	31.42	26.96	27.42	32.96	31.42	26.96	27.42
$t_1$	10-Oct							
$t_2$	24-Oct							
$t_3$	29-Nov	30-Nov	05-Dec	04-Dec	29-Nov	30-Nov	05-Dec	04-Dec

Table 4: Expected value solution, the optimal de-escalation strategy for a single scenario, characterized by the mean contact rates during de-escalation phase 1, 2, and 3.

$c_1$	$c_2$	$c_3$	$\epsilon_0$	$\epsilon_1$	$\epsilon_2$	$\epsilon_3$	$t_1$	$t_2$	$t_3$
7.70	9.95	11.04	143.00	14.04	32.14	37.83	08-Oct	23-Oct	24-Nov

infected cases and the incidence curves remains relatively unchanged, and would remain to be low for five months from May 19 until they start to rise in November.

Fig. 4 shows the histograms of  $\epsilon_0$  generated from a number of simulations. We observe that the resulting  $\epsilon_0$  has values of 146 days within  $\pm 5$  days of differences. We expect the difference will be smaller as we increase the number of scenarios. In the figure, we compare the cases with 8 scenarios and 27 scenarios.

Table 4 shows the optimal strategy evaluated for a single scenario, the scenario consists of the contact rates which are the mean values of the distributions of the contact rates in each of the de-escalation phases. It is called an expected value solution. Note that the resulting  $\epsilon_0 = 143$  (duration of de-escalation phase 0) is less than the one obtained in Table 3,  $\epsilon_0 = 144$ , which considers the various future scenarios. When we incorporate the uncertainties of the various future scenarios, the resulting optimal strategy is to take a conservative option, to have a delayed timing of the next re-opening step which allow us to stay within the health capacity in any of the upcoming scenarios.

Fig. 5 shows the result of using the expected value solution under the uncertainties of contact rates. Contact rates post-re-opening phases are determined by 8 scenarios in Table 3. In the right panel, we observe that the expected number of cases in ICU units would remain under the ICU capacity only for scenario 1 ( $s_1$ , red curve), which projects the lowest contact rates for all de-escalation phases among all scenarios considered. The expected solution is feasible only for scenario 1 ( $s_1$ ) and is not feasible for all other scenarios ( $s_2 - s_8$ ). Due to this infeasibility, the cost of using the expected value solution is infinity. Hence the cost difference between the expected value solution and our stochastic programming

Table 5: Optimal de-escalation strategies when the date of vaccine arrival time is assumed to be in March 2021. The 8 scenarios of contact rates are identical to the ones presented in Table 3.

	$s_1$	$s_2$	$s_3$	$s_4$	$s_5$	$s_6$	$s_7$	$s_8$
$c_{1,r}$	7.55	8.12	7.55	8.12	7.55	8.12	7.55	8.12
$c_{2,r}$	9.90	9.90	10.09	10.09	9.90	9.90	10.09	10.09
$c_{3,r}$	10.99	10.99	10.99	10.99	11.18	11.18	11.18	11.18
$\epsilon_0$	192.94	192.94	192.94	192.94	192.94	192.94	192.94	192.94
$\epsilon_1$	14.00	14.17	14.00	14.17	14.00	14.17	14.00	14.17
$\epsilon_2$	37.74	39.33	44.82	44.09	37.74	39.33	44.82	44.09
$\epsilon_3$	41.32	39.56	34.24	34.80	41.32	39.56	34.24	34.80
$t_1$	27-Nov							
$t_2$	11-Dec	12-Dec	11-Dec	12-Dec	11-Dec	12-Dec	11-Dec	12-Dec
$t_3$	18-Jan	20-Jan	25-Jan	25-Jan	18-Jan	20-Jan	25-Jan	25-Jan

Table 6: Optimal de-escalation strategies with enhanced contact tracing ( $q_r = 0.5$ ). Each of the  $\epsilon_1$ ,  $\epsilon_2$  and  $\epsilon_3$  represents the duration (in days) of de-escalation phase 0, 1 and 2, respectively. Calendar dates presented in the rows of  $t_1$ ,  $t_2$ ,  $t_3$  correspond to the date of initiating de-escalation phase 1, 2 and 3, in the year of 2020.

	$s_1$	$s_2$	$s_3$	$s_4$	$s_5$	$s_6$	$s_7$	$s_8$
$c_{1,r}$	7.55	8.12	7.55	8.12	7.55	8.12	7.55	8.12
$c_{2,r}$	9.90	9.90	10.09	10.09	9.90	9.90	10.09	10.09
$c_{3,r}$	10.99	10.99	10.99	10.99	11.18	11.18	11.18	11.18
$\epsilon_0$	76.76	76.76	76.76	76.76	76.76	76.76	76.76	76.76
$\epsilon_1$	14.00	14.03	14.00	14.03	14.00	14.03	14.00	14.03
$\epsilon_2$	60.85	64.25	74.74	73.50	60.85	64.25	74.74	73.50
$\epsilon_3$	75.38	71.96	61.50	62.71	75.38	71.96	61.50	62.71
$t_1$	3-Aug							
$t_2$	17-Aug							
$t_3$	17-Oct	21-Oct	31-Oct	30-Oct	17-Oct	21-Oct	31-Oct	30-Oct

solution is infinity.

Table 5 show the optimal strategy with a different assumption of the vaccine arrival time, which is delayed for two more months compared with the vaccine arrival time assumed in the simulation for Fig. 2. The two months of delay in the vaccine arrival time resulted in a longer duration of the de-escalation phase 0 and phase 2, while the length of de-escalation phase 1 remains at the minimum length.

With the increased level of contact tracing, initiation timings of de-escalation phase 3 ( $t_3$ ) are expected to be earlier. An example in Table 6 and Fig. 6 shows that if 50% of exposed individuals are quarantined, school re-opening can be in October, instead of in November/December (as shown in Table 3 with lower quarantined proportion,  $q_r = 0.3741$ ). However, the curves of incidence and deaths remain to be similar to the ones with lower quarantined proportion (see Fig. 7 and Fig. 3).

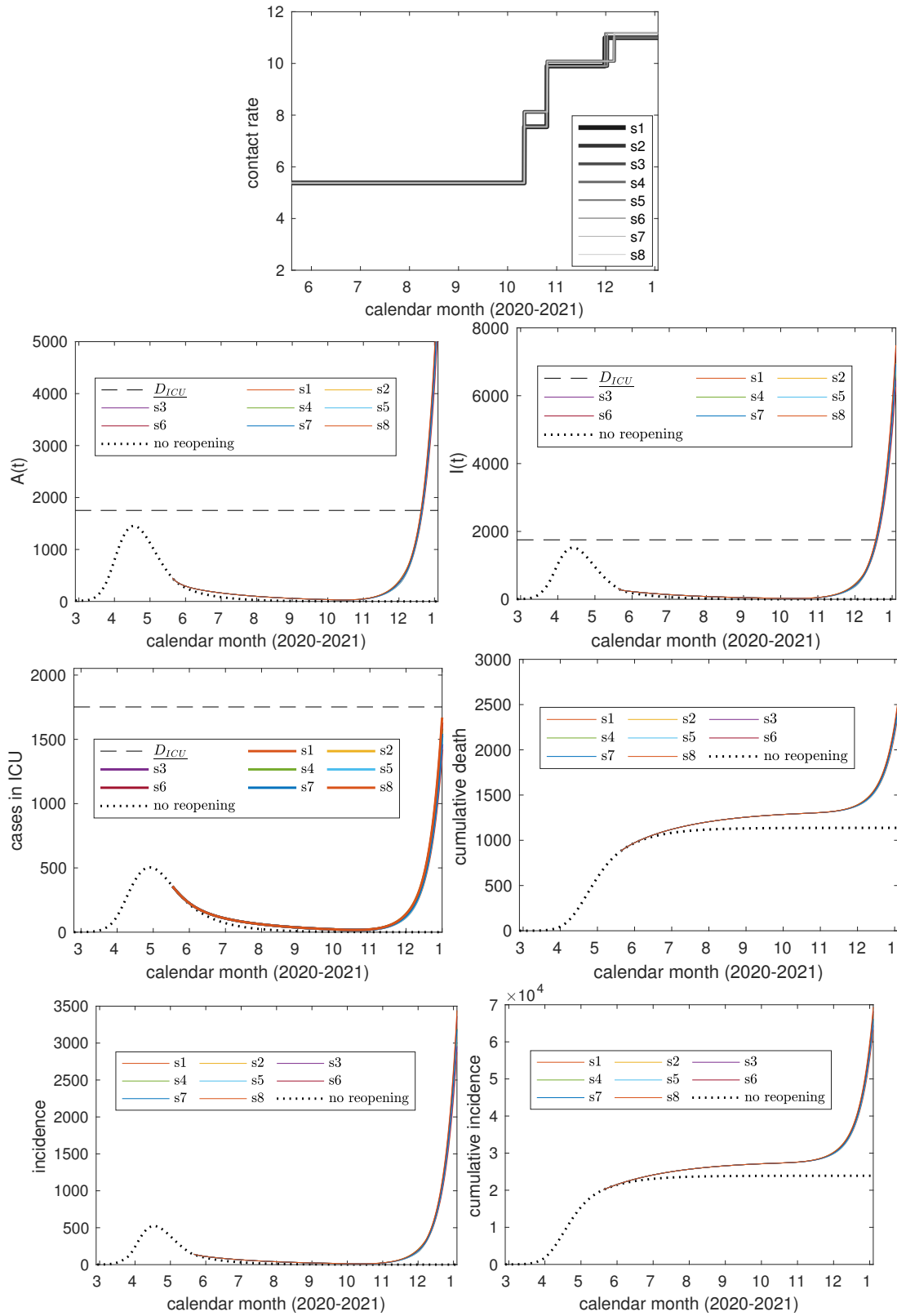


Figure 3: Various scenarios of contact rates and the projected number of cases and deaths during 4 de-escalation phases with a strategy presented in Table 3.

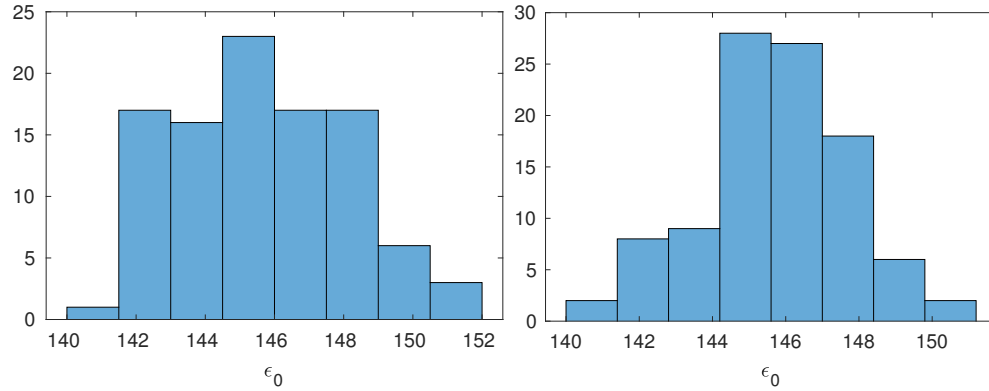


Figure 4: Histograms of  $\epsilon_0$ , the duration of de-escalation phase 0, resulting from 100 simulations. Left (Right) panel shows the result with 8 (27) scenarios. Mean value of  $\epsilon_0$  with 27 scenarios is 145.79.

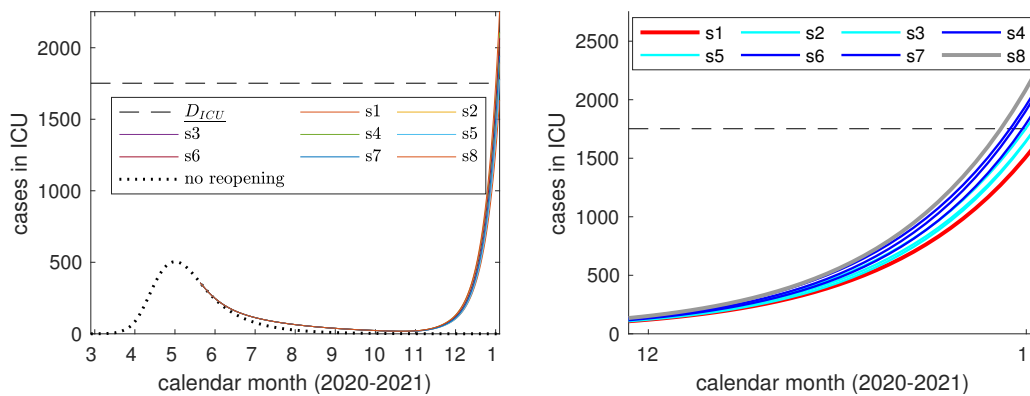


Figure 5: Projected numbers of cases in ICU of the alternative approach, the expected value approach in Table 4 under the 8 scenarios given in the first three rows of Table 3. The right panel shows the curves near the vaccine arrival time in January 2021.

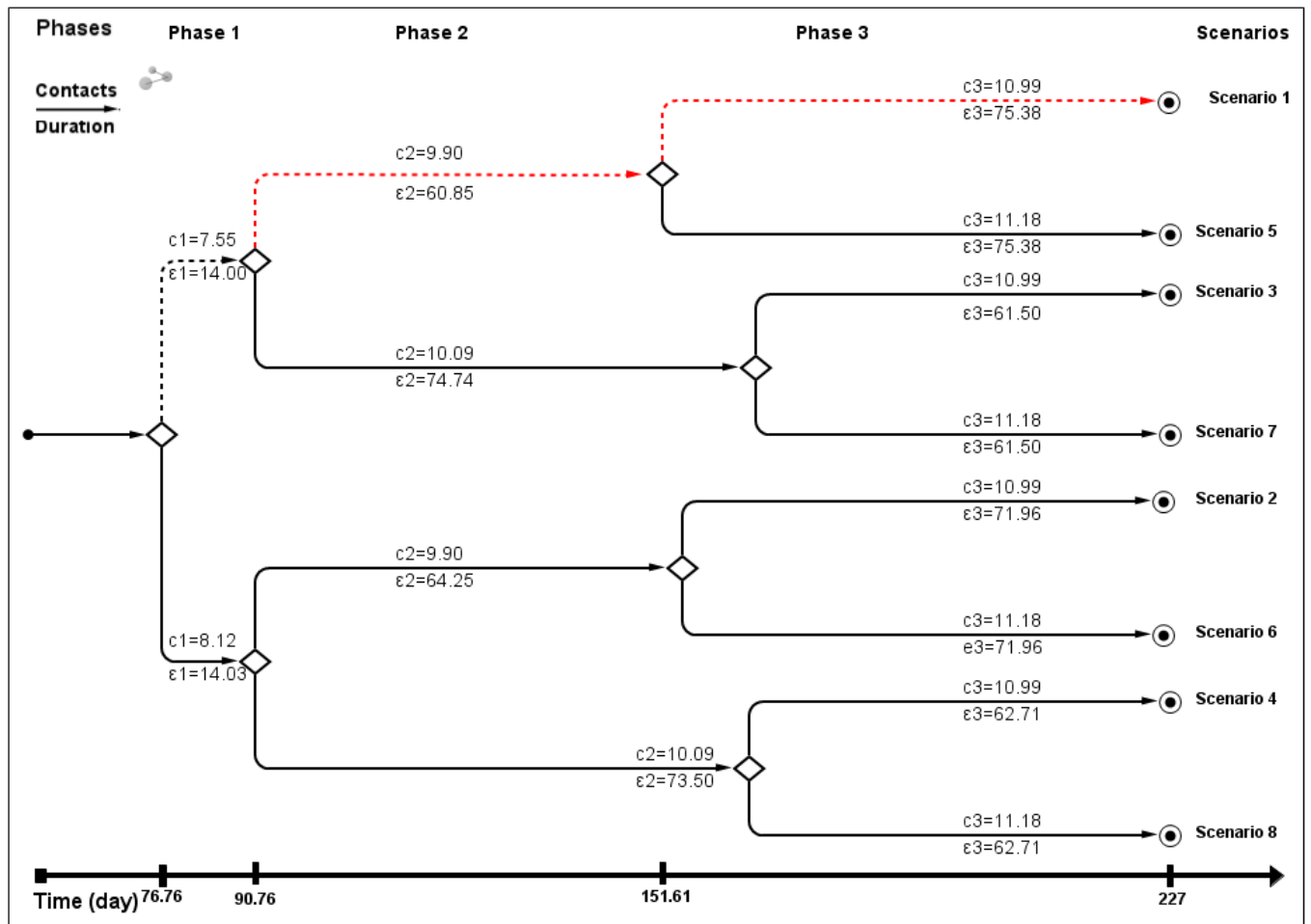


Figure 6: A scenario tree with enhanced contact tracing ( $q_r = 0.5$ ). The 8 scenarios and the optimal strategy are presented in Table 6.

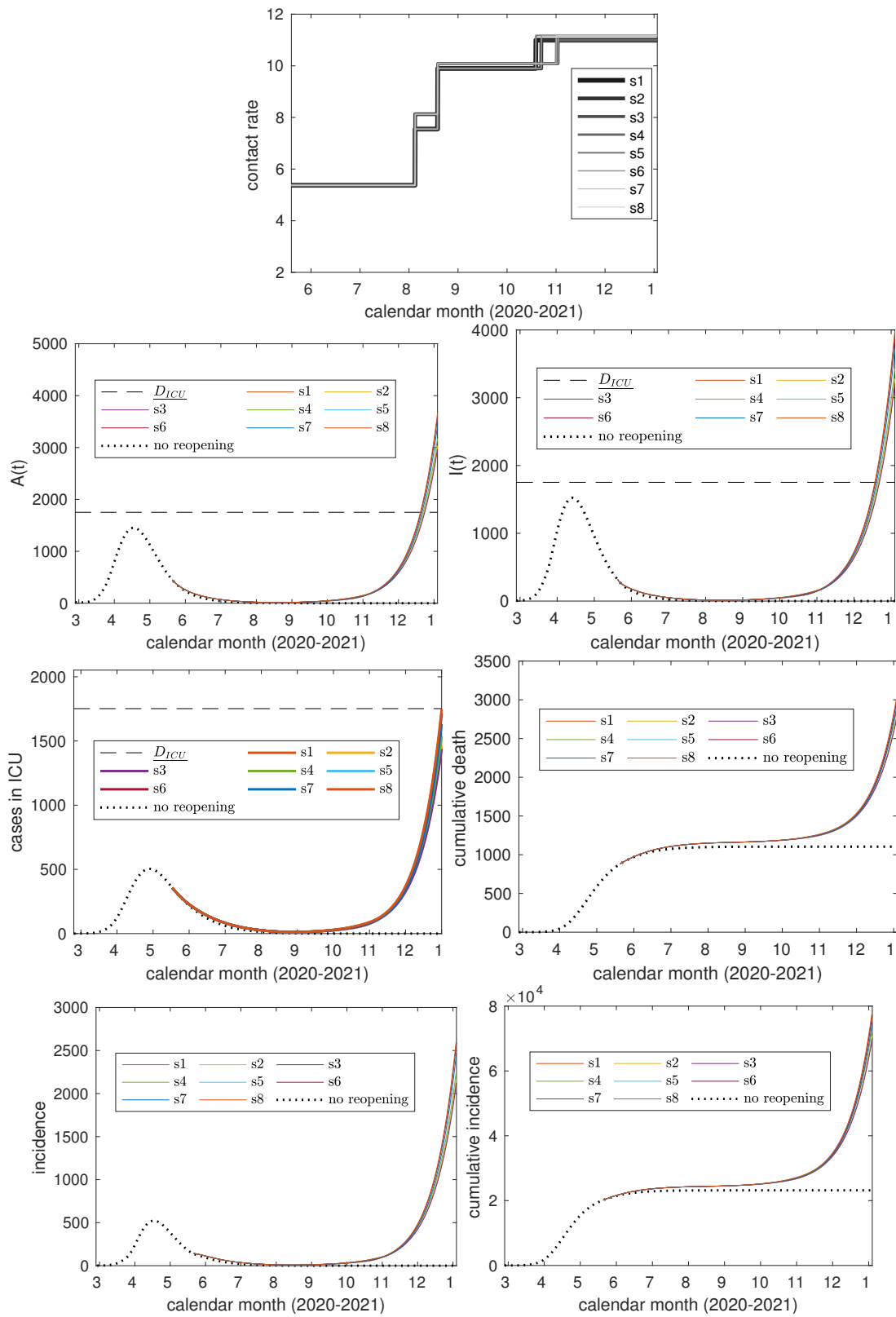


Figure 7: Various scenarios of contact rates and the projected number of cases and deaths with enhanced contact tracing ( $q_r = 0.5$ ).

#### 4. Discussion

In the existing scholarly literature, a few mathematical models have attempted to project COVID-19 related infections, hospitalizations and deaths during the re-opening phase, under various assumptions and scenarios.

For instance, Crawford and colleagues [6] have modelled a slow and a fast re-opening scenario in Connecticut, one of the USA states most hard-hit by the pandemic. In the former scenario, infections are expected to peak by late Summer (mid-August), while in the latter scenario a second peak is anticipated to occur by late Fall. Projected hospitalizations are not expected to exceed bed capacity in both scenarios, even though they could strain the healthcare facilities in the fast re-opening scenario under the assumption of a high fraction of asymptomatic cases. Finally, always under this assumption, deaths could surge in the short-term but should stabilize and be lower in the long-term with respect to the assumption of a low fraction of asymptomatic cases.

Liu and coworkers [8] have devised a SIR model integrated by demographic and mobility data to simulate the spread of COVID-19 in the USA when restrictions are eased. Authors found that counties characterized by the lowest population density could not experience a surge in infections also when public health measures like social distancing are lifted, even though generally in the USA a dramatic peak of cases could occur if social distancing is completely abolished. From a quantitative standpoint, Zhou [27] has estimated an increase in daily confirmed COVID-19 cases by 40%, 52%, and 53% after the first, second, and third week of re-opening, respectively.

Zhao and Feng [26] also used SEIR-type epidemic models to analyze the effects of releasing different age/risk groups in different timings. By comparing several release scenarios, authors were able to quantify benefits of staggered release compared with simultaneous-release policies in terms of risks of venerable population and the disease burden in the overall population.

In the UK, Panovska-Griffiths and collaborators [12] developed a stochastic individual-based model to simulate different lockdown exit strategies. Authors found that relaxing closures that aim to control COVID-19 would result in a rebound/second wave, which can be controlled by a package of integrated public health measures, including expanding testing, contact tracing, diagnosis, and isolation of symptomatic individuals. A similar conclusion was reached by Anderson and coauthors, who devised a Bayesian epidemiological model and found that caution should be taken during the re-opening phase, both when re-opening borders and resuming economic-activities and businesses. A strict monitoring of COVID-19 transmission should be conducted during the relaxation of the public health interventions implemented and enforced during the lockdown.

McBryde and coworkers [9] modelled lockdown exit strategy in Australia utilizing age-based contact matrices, and simulating resumption of different activities (re-opening of workplace and schools). Authors investigated the effects of both micro- and macro-distancing on the SARS-CoV-2 reproduction number.

Finally, Hazem and colleagues [7] have assessed the effect of relaxing the lockdown related restrictions in a number of countries, including the USA, Germany, the UK, Italy,

Spain, and Canada, exploiting a modified SIR model. Authors showed that, even within different scenarios and under various assumptions, a second wave is very likely to occur. Moreover, authors predicted the number of infections for different re-opening dates, under various lockdown exit strategies and found that an optimal strategy would begin easing the public health measures at least 3 months after the turning point of the epidemic curve. Specifically concerning Canada, authors predicted a second wave up to 80 thousand infected cases in case of re-opening on June 1, which could be reduced by 45 percent if postponing re-opening to July 1 (55 thousand infections).

In line with the literature, our study attempted to assess re-opening strategies with the aim of informing public health policy-makers in their decision-making process. Similarly, Cetin and collaborators [5] have built two optimization models, namely a personal protection and a mass protection model, for making cost effective decisions against COVID-19. However, our optimization model has different focuses on the underlying transmission process and the dynamics of the decision process which is adapted to the sequentially revealed uncertainty in future. In more detail, we have developed a novel framework to identify the optimal timing of the upcoming re-opening phase taking account of the randomness in the contact rate during post re-opening phases. This framework is designed to assist adaptive decision process.

For the special case of re-opening strategies in Ontario, Canada, our model has found that the outcomes of the epidemic generated from the optimal strategy would remain to be similar regardless of the future scenario reflecting the randomness in the contact rates. Without the enhancement of other control methods, the optimal duration of de-escalation phase 0 (first part of workplace resumption) would be fairly long, while the duration of succeeding de-escalation phases are shorter. Comparing our results with the expected value solution, we also found that neglecting the uncertainties in future contact behavior would yield an earlier optimal re-opening timing, however, this would result in exceeding the health care capacity. Finally, we mention that our developed framework can be modified to incorporate other uncertainties; for example, the date of effective therapeutics/vaccine becoming available can be incorporated as a random variable.

In our study, the targeted optimization is to minimize the total number of daily average contact rates for all residents in the considered region (here the Province of Ontario, Canada). Decisions on re-opening involve heavily social economic considerations, where values of “contacts” are age-specific and location (household, workplace, school, community) setting-specific. To construct a realistic targeted optimization function that incorporates these social and economic considerations, we must first of all expand the transmission dynamics model in a homogeneous population to age-stratified transmission models with appropriate contact-mixing in the population, and then estimate the values of “contacts” for different age-groups, different contact settings, and for different sectors.

### Acknowledgements

This project has been partially supported by the Canadian Institute of Health Research (CIHR) 2019 Novel Coronavirus (COVID-19) rapid research program. JW is a member of

the Ontario COVID-19 Modelling Consensus Table, and a member of the Expert Panel of the Public Health Agency of Canada (PHAC) Modeling group. This research was presented to both Ontario Table and PHAC group, and we appreciate very much comments and suggestions from colleagues of these provincial table and federal group. Reported COVID-19 cases were obtained from the Public Health Ontario (PHO) integrated Public Health Information System (iPHIS), via the Ontario COVID-19 Modelling Consensus Table.

### References

- [1] Government of Ontario, Ontario significantly expands hospital capacity to prepare for any COVID-19 outbreak scenario. <https://news.ontario.ca/opo/en/2020/04/ontario-significantly-expands-hospital-capacity-to-prepare-for-any-covid-19-outbreak-scenario.html>. Accessed: 2020-05-19.
- [2] PHAC corona virus disease 2019 (COVID-19) daily epidemiology update. <https://health-infobase.canada.ca/covid-19/epidemiological-summary-covid-19-cases.html>. Accessed: 2020-05-11.
- [3] Sergio Arregui, Alberto Aleta, Joaquín Sanz, and Yamir Moreno. Projecting social contact matrices to different demographic structures. *PLoS computational biology*, 14(12):e1006638, 2018.
- [4] John R Birge and Francois Louveaux. *Introduction to stochastic programming*. Springer Science & Business Media, 2011.
- [5] Eyup Cetin, Serap Kiremitci, and Baris Kiremitci. Developing optimal policies to fight pandemics and COVID-19 combat in the United States. *European Journal of Pure and Applied Mathematics*, 13(2), 2020.
- [6] Forrest W. Crawford, Zehang Richard Li, and Olga Morozova. COVID-19 projections for reopening connecticut. *medRxiv*, 2020.
- [7] Yara Hazem, Suchitra Natarajan, and Essam Berikaa. Hasty reduction of COVID-19 lockdown measures leads to the second wave of infection. *medRxiv*, 2020.
- [8] Meng Liu, Raphael Thomadsen, and Song Yao. Forecasting the spread of COVID-19 under different reopening strategies. *medRxiv*, 2020.
- [9] Emma Sue McBryde, James M Trauer, Adeshina Adekunle, Romain Ragonnet, and Michael T Meehan. Stepping out of lockdown should start with school re-openings while maintaining distancing measures. insights from mixing matrices and mathematical models. *medRxiv*, 2020.
- [10] Seyed M Moghadas, Affan Shoukat, Meagan C Fitzpatrick, Chad R Wells, Pratha Sah, Abhishek Pandey, Jeffrey D Sachs, Zheng Wang, Lauren A Meyers, Burton H Singer, et al. Projecting hospital utilization during the COVID-19 outbreaks in the

- United States. *Proceedings of the National Academy of Sciences*, 117(16):9122–9126, 2020.
- [11] Jol Mossong, Hens Niel, Mark Jit, Philippe Beutels, Kari Auranen, Rafael Mikolajczyk, Marco Massari, Salmaso Stefania, Gianpaolo Scalia Tomba, Jacco Wallinga, Janneke Heijne, Malgorzata Sadkowska-Todys, Rosinska Magdalena, and John W Edmunds. Social contacts and mixing patterns relevant to the spread of infectious diseases. *PLoS medicine*, 5(3):e74, 2008.
- [12] Jasmina Panovska-Griffiths, Cliff Kerr, Robyn Margaret Stuart, Dina Mistry, Daniel Klein, Russell M Viner, and Chris Bonell. Determining the optimal strategy for reopening schools, work and society in the uk: balancing earlier opening and the impact of test and trace strategies with the risk of occurrence of a secondary COVID-19 pandemic wave. *medRxiv*, 2020.
- [13] Kiesha Prem, Alex R Cook, and Mark Jit. Projecting social contact matrices in 152 countries using contact surveys and demographic data. *PLoS computational biology*, 13(9):e1005697, 2020.
- [14] Chiara Reno, Jacopo Lenzi, Antonio Navarra, Eleonora Barelli, Davide Gori, Alessandro Lanza, Riccardo Valentini, Biao Tang, and Maria Pia Fantini. Forecasting COVID-19-associated hospitalizations under different levels of social distancing in lombardy and emilia-romagna, northern italy: Results from an extended seir compartmental model. *Journal of Clinical Medicine*, 9(5):1492, 2020.
- [15] Steven Sanche, Yen Ting Lin, Chonggang Xu, Ethan Romero-Severson, Nicolas W Hengartner, and Ruian Ke. The novel coronavirus, 2019-nCoV, is highly contagious and more infectious than initially estimated. *arXiv preprint arXiv:2002.03268*, 2020.
- [16] Affan Shoukat, Chad R Wells, Joanne M Langley, Burton H Singer, Alison P Galvani, and Seyed M Moghadas. Projecting demand for critical care beds during COVID-19 outbreaks in Canada. *CMAJ*, 192(19):E489–E496, 2020.
- [17] Biao Tang, Nicola Luigi Bragazzi, Qian Li, Sanyi Tang, Yanni Xiao, and Jianhong Wu. An updated estimation of the risk of transmission of the novel coronavirus (2019-ncov). *Infectious disease modelling*, 5:248–255, 2020.
- [18] Biao Tang, Francesca Scarabel, Nicola Luigi Bragazzi, Zachary McCarthy, Michael Glazer, Yanyu Xiao, Jane M Heffernan, Ali Asgary, Nicholas Hume Ogden, and Jianhong Wu. De-escalation by reversing the escalation with a stronger synergistic package of contact tracing, quarantine, isolation and personal protection: Feasibility of preventing a COVID-19 rebound in Ontario, Canada, as a case study. *Biology*, 9(5):100, 2020.
- [19] Biao Tang, Xia Wang, Qian Li, Nicola Luigi Bragazzi, Sanyi Tang, Yanni Xiao, and Jianhong Wu. Estimation of the transmission risk of the 2019-ncov and its implication for public health interventions. *Journal of clinical medicine*, 9(2):462, 2020.

- [20] Biao Tang, Fan Xia, Nicola Luigi Bragazzi, Xia Wang, Sha He, Xiaodan Sun, Sanyi Tang, Yanni Xiao, and Jianhong Wu. Lessons drawn from China and South Korea for managing COVID-19 epidemic: insights from a comparative modeling study. *Bulletin of the World Health Organization*, 2020.
- [21] Biao Tang, Fan Xia, Sanyi Tang, Nicola Luigi Bragazzi, Qian Li, Xiaodan Sun, Juhua Liang, Yanni Xiao, and Jianhong Wu. The effectiveness of quarantine and isolation determine the trend of the COVID-19 epidemics in the final phase of the current outbreak in china. *International Journal of Infectious Diseases*, 2020.
- [22] Ashleigh R Tuite, David N Fisman, and Amy L Greer. Mathematical modelling of COVID-19 transmission and mitigation strategies in the population of ontario, canada. *CMAJ*, 192(19):E497–E505, 2020.
- [23] Ashleigh R Tuite, Amy L Greer, Steven De Keninck, and David N Fisman. Risk for COVID-19 resurgence related to duration and effectiveness of physical distancing in ontario, canada. *Annals of Internal Medicine*, 2020.
- [24] Jianhong Wu, Biao Tang, Nicola Luigi Bragazzi, Kyeongah Nah, and Zachary McCarthy. Quantifying the role of social distancing, personal protection and case detection in mitigating COVID-19 outbreak in Ontario, Canada. *Journal of Mathematics in Industry*, 10(1):1–12, 2020.
- [25] Yanyu Xiao, LIAM-ADERSIM De escalation Task Force, and Jianhong Wu. Estimation of age-specific and daily average contact rates under different reopening strategies and their implication for controlling COVID-19 resurgences. *In preparation*, 2020.
- [26] Henry Zhao and Zhilan Feng. Staggered release policies for COVID-19 control: Costs and benefits of relaxing restrictions by age and risk. *Mathematical biosciences*, page 108405, 2020.
- [27] Qiyao Zhou. The effect of reopening policy on covid-19 related cases and deaths. *medRxiv*, 2020.